

LLMs Uncertainty Quantification via Adaptive Conformal Semantic Entropy

Hamed Karimi¹, Vaishali Meyappan¹, Reza Samavi^{1,2}

¹ Toronto Metropolitan University, Toronto, Ontario, Canada

² Vector Institute, Toronto, Ontario, Canada

{hamed.karimi, vaishali.meyappan, samavi}@torontomu.ca

Abstract

LLMs’ overconfidence, particularly when hallucinating, poses a significant challenge for the deployment of the models in safety-critical settings and makes a reliable estimation of uncertainty necessary. Existing approaches for uncertainty quantification typically prioritize lexical or probabilistic measures; however, these techniques often ignore the semantic variance of different responses with similar meaning. In this paper, we propose Adaptive Conformal Semantic Entropy (ACSE), a method for estimating prompt-level uncertainty by adaptively measuring semantic dispersion in LLMs outputs. Our uncertainty scoring function is based on clustering semantic entropy of multiple diverse responses to the same prompt. The function adaptively adjusts the uncertainty score based on semantic features of each cluster. To ensure statistical reliability of our score, we use conformal calibration to apply a decision rule to accept/abstain the prompts, providing a finite-sample, distribution-free guarantee such that the error rate among the accepted responses remains bounded by a user-specified tolerance. Our extensive experimental evaluations using different LLMs and datasets, demonstrate that our approach consistently outperforms state-of-the-art uncertainty quantification baselines using discriminative performance, conformal guarantees, and probabilistic calibration indicators. As a highlight, for TriviaQA dataset, AUROC of our approach is 0.88 compared to 0.65 produced by the token entropy approach.

1 Introduction

Despite the wide range application of Large Language Models (LLMs), they remain uncertain in their predictions and often generate incorrect or misleading outputs with high confidence [Shanahan, 2024]. This overconfidence limits their safe deployment in high-stakes domains such as healthcare [Thirunavukarasu *et al.*, 2023], law [Teubner *et al.*, 2023], and scientific research [Liu *et al.*, 2023]. Reliable uncertainty quantification (UQ), defined as the process of estimating the model’s confidence in its own predictions, is therefore essen-

tial for improving model reliability, safety, and trustworthiness [Chang *et al.*, 2024].

Related Work. Most existing methods for uncertainty estimation in LLMs rely on token-level signals, such as entropy over next-token distributions [Duan *et al.*, 2023; Fadeeva *et al.*, 2024; Yarie *et al.*, 2024] or average sequence log-likelihood [Yao *et al.*, 2019; Huang *et al.*, 2023]. While computationally efficient, these approaches capture only surface-level lexical variability rather than uncertainty over meaning [Shorinwa *et al.*, 2025]. In autoregressive generation, LLMs often assign high probability to multiple near-synonymous tokens, producing outputs that are probabilistically coherent yet semantically ambiguous or incorrect. As a result, token-level entropy cannot distinguish superficial phrasing variation from genuine semantic ambiguity. In particular, entropy may remain low even when probability mass is spread across responses with mutually inconsistent meanings, creating a misleading impression of confidence [Brown *et al.*, 2020; Holtzman *et al.*, 2020].

More recent work has shifted toward semantic-level uncertainty estimation, notably Semantic Entropy (SE) [Kuhn *et al.*, 2023], which aggregates uncertainty by clustering semantically equivalent responses using Natural Language Inference. However, SE relies on hard cluster assignments, forcing each response into a single cluster and ignoring overlapping semantic regions, which can yield unstable uncertainty estimates. To improve reliability, conformalized approaches [Kaur *et al.*, 2024] employ dynamic clustering with finite-sample guarantees, while the Conformalized Abstention Policy [Tayebati *et al.*, 2025] integrates reinforcement learning to learn instance-specific risk thresholds. Despite their guarantees, these methods treat uncertainty as a scalar signal and remain insensitive to cluster brittleness. As a result, they are vulnerable to the wrong-consensus trap, in which lexically consistent but factually incorrect response clusters satisfy conformal thresholds, masking underlying semantic error.

Proposal. To address these limitations, we propose *Adaptive Conformal Semantic Entropy* (ACSE), a model-independent method that quantifies uncertainty in pretrained LLMs based on dispersion in meaning. Rather than relying on token-level signals, ACSE estimates prompt-level uncertainty in a continuous semantic vector space, capturing dispersion in response meaning. For a finite set of representative prompts (e.g.,

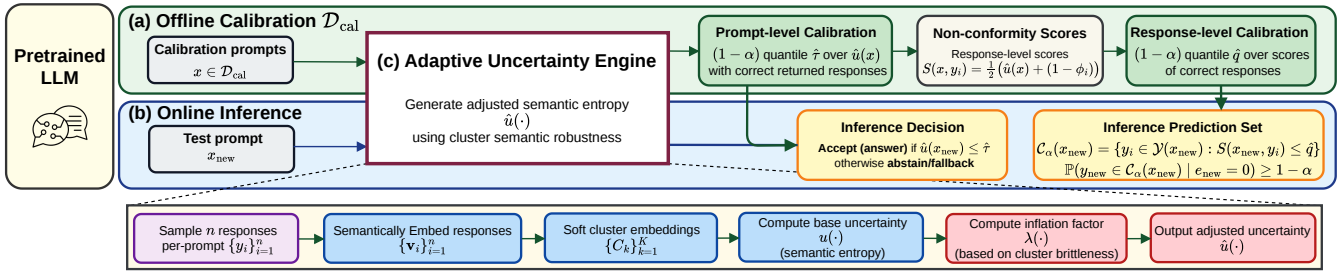


Figure 1: ACSE Pipeline. (a) To calibrate a pretrained LLM, for each prompt $x \in \mathcal{D}_{\text{cal}}$, we use an Adaptive Uncertainty Engine (AUE) to compute an adjusted uncertainty score, $\hat{u}(x)$. The $\hat{u}(x)$ is then used to compute a cutoff for a conformalized decision rule (prompt-level) and prediction set in response-level for the user defined upper bound error guarantee of α . (b) In inference time, for a new prompt, the same AUE is used to compute $\hat{u}(x)$ to compare with the calibration cutoff. (c) AUE starts with sampling n responses, embeds them, and soft-clusters the embeddings, leading to the computation of base semantic entropy $u(x)$.

1,000 calibration prompts), we sample multiple responses per prompt, embed each response using a sentence encoder whose cosine similarity reflects semantic proximity [Reimers and Gurevych, 2019], and cluster the embeddings into coherent semantic groups. We then estimate probability mass for each group via soft assignments and derive a base uncertainty score from the normalized entropy of the resulting distribution. This base semantic uncertainty reflects the degree of meaning dispersion: higher dispersion—corresponding to multiple semantically distinct responses—indicates greater uncertainty, whereas semantically consistent responses imply lower uncertainty [Yadkori *et al.*, 2024]. We subsequently adjust the uncertainty score when cluster structure indicates brittleness, such as weak support for the dominant cluster, high internal diversity, or other risk patterns that empirically correlate with errors under distribution shift. Finally, we calibrate the adjusted uncertainty score using conformal prediction on held-out calibration prompts [Vovk *et al.*, 2005] to learn a cutoff that serves two purposes: (1) making prompt-level answer/abstain decisions and (2) generating response-level prediction sets to support user decision-making. Figure 1 provides an overview of the approach, which is illustrated by a toy example.

Toy Example. Consider a user querying a pretrained geographical LLM with the prompt *What is the capital of Australia?*. The model returns *Sydney* with probability 70% (high confidence) despite its semantic incorrectness, and *Canberra* with probability 30% (low confidence). Selecting the most likely sequence yields a *wrong consensus*, a common failure mode in open-ended generation. Assume the user has calibrated the model on a held-out set of geographical prompts and identified 0.58 as a conformity cutoff corresponding to 90% confidence under the assumption that new prompts are drawn from the same distribution [Vovk *et al.*, 2005]. For a new prompt, ACSE samples 10 responses using fixed decoding settings: 9 contain *Sydney* and 1 contains *Canberra*. These responses are embedded, clustered by meaning, and assigned soft semantic memberships via normalized cosine similarity to cluster centroids. Since assignments are probabilistic, clusters are non-disjoint. Averaging memberships across responses yields mean cluster weights of 0.87 for *Sydney* and 0.13 for *Canberra*. The resulting base semantic uncertainty score, given by the normalized entropy of these weights, is

0.55. Because this score falls below the abstention threshold (0.55 < 0.58), the model would return the dominant *Sydney* cluster. However, semantic entropy alone can be overly optimistic when clusters are internally brittle, e.g., when cluster membership is unstable or weakly representative. Our approach accounts for such brittleness by adjusting the uncertainty score. In this example, incorporating cluster quality factors (Section 3.1) increases the score to 0.62. Since 0.62 > 0.58, the model abstains from returning the incorrect answer. While sampling and post-processing incur additional cost, this overhead is justified in safety-critical applications such as using LLMs for mental health support.

Contributions. We make the following contributions. First, we propose ACSE, a method for estimating entropy-based uncertainty at the semantic level for a given prompt. Second, we introduce an adjusted uncertainty score that leverages cluster robustness features to adaptively inflate semantic uncertainty, explicitly penalizing ambiguous response semantics and mitigating hallucinations. Third, we incorporate a post-hoc conformal calibration phase on held-out prompts to learn a cutoff over adjusted uncertainty estimates aligned with response correctness and with formal guarantee, yielding decision rules in both prompt-level and response level. Finally, we demonstrate through extensive experiments on open-domain question answering benchmarks that our adaptive semantic-level uncertainty modeling achieves superior discrimination and calibration compared to state-of-the-art baselines.

2 Prompt-Level Uncertainty Estimation

ACSE calibrates a pretrained LLM to a new domain using a finite set of labeled calibration prompts \mathcal{D}_{cal} of size M . Calibration begins by sampling multiple responses per prompt to assess the consistency of the model’s generated meanings.

2.1 Response Sample Generation

Let \mathcal{V} denote the token vocabulary. A generated response is a finite token sequence $y_i = \langle y_{i,1}, \dots, y_{i,T_i} \rangle$ terminated by an EOS token in T_i decoding steps. For a fixed input prompt $x \in \mathcal{X}$, we draw a set of n independent responses $\mathcal{Y}(x) = \{y_1, \dots, y_n\}$ from a language model with parameters θ . At each decoding step t , the model defines a next-token

probability distribution over tokens $v \in \mathcal{V}$ as,

$$\pi_{i,t}(v) = p_\theta(y_{i,t} = v \mid x, y_{i,1:t-1}), \quad \sum_{v \in \mathcal{V}} \pi_{i,t}(v) = 1, \quad (1)$$

where $y_{i,t}$ denotes the t -th token of response y_i . To balance diversity and semantic coherence, we adopt nucleus (top- η) sampling [Holtzman *et al.*, 2020], which dynamically truncates the distribution at each step. Specifically, the nucleus $\Gamma_\eta(x, i, t)$ is the smallest subset of tokens whose cumulative probability exceeds a threshold $\eta \in \mathbb{R}^{(0,1]}$,

$$\Gamma_\eta(x, i, t) = \arg \min_{L \subseteq \mathcal{V}} \left\{ |L| : \sum_{v \in S} \pi_{i,t}(v) \geq \eta \right\}. \quad (2)$$

The truncated distribution is obtained by renormalizing over Γ_η ,

$$\pi_{i,t}^{(\eta)}(v) = \begin{cases} \frac{\pi_{i,t}(v)}{\sum_{v \in \Gamma_\eta(x, i, t)} \pi_{i,t}(v)}, & v \in \Gamma_\eta(x, i, t), \\ 0, & \text{otherwise.} \end{cases} \quad (3)$$

Tokens are sampled as $y_{i,t} \sim \pi_{i,t}^{(\eta)}(\cdot)$ and appended until EOS or a length limit is reached. Repeating this procedure yields the response set $\mathcal{Y}(x)$. The variability of $\mathcal{Y}(x)$ provides an empirical proxy for model confidence. When the model is confident, stochastic decoding produces lexically diverse but semantically equivalent responses; when uncertain, samples diverge into multiple, often conflicting, meanings. The sample size n controls a trade-off between computational cost and resolution: larger n captures finer-grained semantic variation, while smaller n suffices when responses concentrate on a single meaning. In the next step, we quantify this dispersion by embedding $\mathcal{Y}(x)$ into a semantic space where cosine similarity reflects semantic proximity.

2.2 Semantic Embedding

We represent each sampled response by its underlying meaning rather than its surface form, so that paraphrases are embedded nearby while semantically distinct answers are well separated. This representation enables reliable grouping of responses into semantic clusters for downstream uncertainty estimation. Each generated response $y_i \in \mathcal{Y}(x)$ is mapped into a continuous semantic space using a pre-trained sentence encoder $f : \mathcal{Y} \rightarrow \mathbb{R}^d$, producing embeddings

$$\mathcal{E} = \{ \mathbf{v}_i = f(y_i) \in \mathbb{R}^d \mid y_i \in \mathcal{Y}(x) \}. \quad (4)$$

We ℓ_2 -normalize these embeddings such that $\|\mathbf{v}_i\|_2 = 1$ and measure similarity using cosine geometry [Cer *et al.*, 2018; Reimers and Gurevych, 2019; Gao *et al.*, 2021]. This choice reflects semantic relatedness across lexical and syntactic variation, provides bounded and scale-invariant similarity scores, and yields more stable neighborhoods in high-dimensional spaces than Euclidean distance. The resulting embeddings capture the latent semantic structure of model outputs and form the basis for measuring dispersion in meaning. The effectiveness of this representation depends on selecting a sentence encoder that reliably separates semantic similarity from surface variation. Using the embeddings \mathcal{E} , we define a binary

error function $e : \mathcal{X} \times \mathcal{Y} \rightarrow \{0, 1\}$ that assigns error labels to prompt-response pairs where $e(x, y_i) = \mathbb{1}\{y_i \text{ is incorrect}\}$. Labels are determined automatically via semantic matching [Cer *et al.*, 2018; Reimers and Gurevych, 2019]. Given a reference response \hat{y} for prompt x and a cosine similarity threshold $\tau_{\text{cos}} \in (0, 1)$, a response y_i is labeled correct if $\cos(\mathbf{v}_{y_i}, \mathbf{v}_{\hat{y}}) \geq \tau_{\text{cos}}$. In the following, we leverage semantic clusters of \mathcal{E} to derive soft assignments that preserve the semantic ranking induced by the encoder.

2.3 Soft Clustering of Semantic Embedding

To transform the unstructured distribution of response embeddings into a meaningful uncertainty signal, we aggregate semantically proximal embeddings into clusters that represent distinct meanings. This serves two purposes: (1) collapsing lexically diverse but semantically equivalent responses into a single equivalence class, and (2) exposing higher-level semantic structure whose relative prevalence reflects model uncertainty. We apply Hierarchical Agglomerative Clustering (HAC) [Murtagh and Contreras, 2017] to the embedding set \mathcal{E} under cosine geometry. Using unit-normalized embeddings, cosine dissimilarity reduces to

$$\text{dist}(\mathbf{v}, \hat{\mathbf{v}}) = 1 - \mathbf{v}^\top \hat{\mathbf{v}}, \quad \text{s.t.} \quad \|\mathbf{v}\|_2 = \|\hat{\mathbf{v}}\|_2 = 1. \quad (5)$$

HAC constructs a dendrogram by iteratively merging clusters with minimum average pairwise dissimilarity (average linkage), balancing sensitivity to local neighborhoods and global coherence. Cutting the dendrogram at a threshold $\epsilon \in \mathbb{R}^{(0,1)}$ yields a set of K semantically coherent clusters

$$\mathcal{J} = \{C_1, \dots, C_K\}, \quad \text{where} \quad \bigcup_{k=1}^K C_k = \mathcal{E}. \quad (6)$$

Lower ϵ enforces strict semantic agreement and higher ϵ allows broader conceptual grouping. This adaptive thresholding aligns cluster granularity with the intrinsic density of the embedding space.

To avoid overstating certainty near cluster boundaries, we adopt soft cluster assignments. Each cluster C_k is represented by a centroid $\mathbf{c}_k = \sum_{\mathbf{v} \in C_k} \mathbf{v} / |C_k|$. For a response embedding \mathbf{v}_i , we compute its similarity to each centroid as,

$$a_{ik} = \frac{1}{2} \left(1 + \cos(\mathbf{v}_i, \mathbf{c}_k) \right) \in \mathbb{R}^{[0,1]}, \quad (7)$$

which is a parameter-free, monotonic transformation that preserves angular geometry without temperature tuning. Then, normalizing across clusters yields soft assignments

$$s_{ik} = \frac{a_{ik}}{\sum_{k=1}^K a_{ik}}, \quad \text{s.t.} \quad \sum_{k=1}^K s_{ik} = 1, \quad (8)$$

where s_{ik} quantifies the degree to which response y_i supports semantic cluster C_k . Assignments concentrate when a response aligns strongly with one cluster, and disperse when it lies between competing meanings, preserving signals of semantic ambiguity. Finally, we aggregate soft assignments across the n sampled responses for prompt x to obtain a prompt-level distribution over meanings $\mathcal{P}(C_k) =$

$n^{-1} \sum_{i=1}^n s_{ik}$ where $\sum_{k=1}^K \mathcal{P}(C_k) = 1$. We define the *Semantic Entropy (SE)* as,

$$\mathcal{H}_{\text{sem}}(x) = - \sum_{k=1}^K \mathcal{P}(C_k) \log \mathcal{P}(C_k), \quad (9)$$

and normalize it to ensure comparability across prompts with different K ,

$$u(x) = \begin{cases} \frac{\mathcal{H}_{\text{sem}}(x)}{\log K}, & K \geq 2, \\ 0, & K = 1. \end{cases} \quad (10)$$

The normalized score $u(x) \in \mathbb{R}^{[0,1]}$ quantifies semantic dispersion: low values indicate strong agreement on a single meaning, while high values reflect uncertainty arising from competing semantic interpretations.

3 Conformalized Adaptive Semantic Entropy

Conformal Prediction. Conformal Prediction (CP) is a distribution-free framework for calibrating set-valued predictions with finite-sample guarantees. Given a calibration dataset $\mathcal{D}_{\text{cal}} = \{(x_i, y_i)\}_{i=1}^M$ and a test point (x_{M+1}, y_{M+1}) drawn from the same distribution, CP ensures

$$\mathbb{P}(y_{M+1} \in \mathcal{C}(x_{M+1})) \geq 1 - \alpha, \quad (11)$$

where $\alpha \in \mathbb{R}^{(0,1)}$ is the miscoverage level and \mathcal{C} is the prediction set [Vovk *et al.*, 2005]. CP relies on a non-conformity score $S : \mathcal{X} \times \mathcal{Y} \rightarrow \mathbb{R}^+$ that measures how poorly a candidate output conforms to the calibration data. For confidence level $1 - \alpha$, the prediction set is

$$\mathcal{C}(x) = \{\hat{y} \in \mathcal{Y} : S(x, \hat{y}) \leq \tau_\alpha\}, \quad (12)$$

where τ_α is the empirical $(1 - \alpha)$ -quantile of calibration scores. This guarantee is model- and distribution-agnostic with exchangeability assumption, i.e., the joint distribution is invariant under permutations of the calibration samples. We refer to [Angelopoulos and Bates, 2023] for a comprehensive treatment. We adapt CP calibration to LLMs for two complementary purposes: (1) to derive a prompt-level decision rule that determines whether to answer or abstain, and (2) to construct a response-level prediction set over sampled outputs that supports user decision-making by identifying responses satisfying conformal coverage. Achieving these goals hinges on a critical component of CP: the fidelity of the non-conformity score. Since the quality of conformal prediction sets depends directly on this score, we introduce an adjusted uncertainty score tailored to LLMs (Section 3.1).

3.1 Adjusted Semantic Uncertainty

Although the base semantic uncertainty $u(x)$ in (10) captures dispersion across meanings, it does not account for structural properties of semantic clusters that correlate with prediction difficulty. In particular, $u(x)$ can underestimate uncertainty in low-sample regimes, semantically heterogeneous clusters with weak separation, and sparsely supported clusters that are vulnerable to distribution shift. To address this, we amplify $u(x)$ using the *odds of uncertainty*, $O(u, x) = u(x)/(1 - u(x))$,

which represents the uncertainty-confidence ratio. To capture cluster brittleness, we define a prompt-level inflation factor $\lambda : \mathcal{X} \rightarrow \mathbb{R}^{[1, \lambda_{\text{max}}]}$ to scale these odds such that $O(\hat{u}, x) = \lambda(x) \cdot O(u, x)$, leading to the adjusted uncertainty

$$\hat{u}(x) = \frac{\lambda(x) u(x)}{1 + (\lambda(x) - 1) u(x)} \in \mathbb{R}^{[u(x), 1]}. \quad (13)$$

This bounded, monotone, and order-preserving transform ensures $\hat{u}(x) \geq u(x)$ with equality iff $\lambda(x) = 1$ or $u(x) \in \{0, 1\}$. Inflation increases with both u and λ , peaking at intermediate $u(x)$ values to prioritize sensitive borderline decisions. Unlike response-level error labels $e(x, y)$, the inflation factor $\lambda(x)$ operates strictly at the prompt level by aggregating properties of the full response set $\mathcal{Y}(x)$.

To make $\lambda(x)$ interpretable and data-driven, we synthesize five normalized, prompt-level robustness features from the embedding geometry using ℓ_2 -normalized response embeddings $\{\mathbf{v}_i\}_{i=1}^n$, soft assignments s_{ik} of response y_i to cluster C_k , and the agglomerative cluster set \mathcal{J} with unit-norm centroids $\{\mathbf{c}_k\}_{k=1}^K$, where $k^* = \arg \max_k \mathcal{P}(C_k)$ denotes the dominant cluster and $i^* = \arg \max_i s_{ik^*}$ denotes the response most representative of the dominant cluster C_{k^*} .

(1) Semantic Entropy. The normalized semantic entropy $u(x)$ measures multimodality across clusters and serves as the primary ambiguity signal. Larger $u(x)$ directly increases $\lambda(x)$, inflating uncertainty when probability mass is spread across competing meanings.

(2) Centroid Distance. We assess if the dominant response is geometrically supported by its cluster using the centroid similarity $a_{i^*k^*}$ in (7). The distance $\tilde{a}(x) = 1 - a_{i^*k^*}$ is small when the representative response lies near the cluster center and large when it is atypical, indicating structural instability. We set $\tilde{a}(x) \propto \lambda(x)$ so that uncertainty increases whenever the dominant prediction lacks sufficient geometric support.

(3) Dominant Cluster Dispersion. To quantify internal coherence, we define the intra-cluster dispersion

$$d_{k^*}(x) = \frac{1}{2|C_{k^*}|} \sum_{\mathbf{v} \in C_{k^*}} \left(1 - \cos(\mathbf{v}, \mathbf{c}_{k^*})\right) \in \mathbb{R}^{[0,1]}. \quad (14)$$

Low values indicate tight semantic agreement, while high values reflect weak internal consistency; $d_{k^*}(x)$ increases $\lambda(x)$ proportionally; thus, uncertainty is inflated whenever the dominant cluster lacks internal coherence.

(4) Dominant Cluster Size. To penalize fragile consensus supported by few samples, we define the sparsity feature

$$g_{k^*}(x) = \min\left\{1, \frac{\kappa}{|C_{k^*}|}\right\} \in \mathbb{R}^{[0,1]}, \quad (15)$$

where $\kappa = \text{median}_{x \in \mathcal{D}_{\text{cal}}}(\max_k |C_k|)$ is a dataset-specific scaling constant computed once on \mathcal{D}_{cal} . Smaller dominant clusters yield larger $g_{k^*}(x)$ directly proportional to $\lambda(x)$ to inflate uncertainty under sparse semantic support.

(5) Margin to Threshold (Overconfidence Suppression). To suppress unwarranted confidence in the low-uncertainty regime, we introduce the margin-to-threshold feature $m(x)$.

Using the calibration set \mathcal{D}_{cal} , we define a label-free reference threshold $\tau_{\text{ref}} = \text{Quantile}_{\gamma}(\{u(x) : x \in \mathcal{D}_{\text{cal}}\})$ where $\gamma \geq 0.5$ is user specified. This threshold is fixed after calibration and reused during deployment to compute $\lambda(x)$, thereby preserving the validity of subsequent conformal calibration. We define the normalized margin

$$m(x) = \max\left\{0, 1 - \frac{u(x)}{\tau_{\text{ref}}}\right\} \in \mathbb{R}^{[0,1]}, \quad (16)$$

which is large when $u(x) \ll \tau_{\text{ref}}$, indicating extreme, and potentially miscalibrated confidence. We incorporate $m(x)$ into $\lambda(x)$ so that overconfident prompts receive additional inflation, nudging borderline cases toward abstention, while the max operator ensures the penalty vanishes whenever $u(x) \geq \tau_{\text{ref}}$.

All features are computed identically during calibration and inference to ensure representational consistency. The constants κ and τ_{ref} are derived once from the unlabeled calibration set \mathcal{D}_{cal} and frozen thereafter, preserving conformal validity. To design our monotone inflation function λ , we introduce a non-negative weight vector $\mathbf{w} = \langle w_u, w_{\tilde{a}}, w_d, w_g, w_m \rangle \in [0, 1]^5$ that encodes the relative contribution of each structural semantic feature of the feature set $\mathcal{F} = \{u, \tilde{a}, d_{k^*}, g_{k^*}, m\}$ where $\sum_{l \in \mathcal{F}} w_l = 1$. These assigned weights are a design choice and not learned parameters, accounting for prioritization over cluster brittleness features. We aggregate the feature set \mathcal{F} by weighted average, into the normalized composite brittleness metric $B(x) = \sum_{l \in \mathcal{F}} w_l l(x) \in \mathbb{R}^{[0,1]}$ where larger $B(x)$ indicates a less reliable prompt due to cluster brittleness. We then define the inflation mapping

$$\lambda(x) = \frac{2}{2 - B(x)} \in \mathbb{R}^{[1,2]}, \quad (17)$$

which satisfies $\lambda_{\min}(x) = 1$ for benign prompts ($B(x) = 0$) and approaches the bounded maximum $\lambda_{\max}(x) = 2$ under maximal structural brittleness, while remaining strictly increasing and convex in $B(x)$. This yields a smooth convex map from $[0, 1]$ to $[1, 2]$ ensuring boundedness, monotonicity, and order preservation while amplifying high-brittleness cases. Since $\partial\lambda/\partial l > 0$ for all $l \in \mathcal{F}$, any increase in cluster brittleness inflates $\hat{u}(x)$ via (13). As the entire inflation procedure is label-free, conformal calibration and inference remain valid in the transformed \hat{u} -space, preserving finite-sample guarantees.

3.2 Prompt Acceptance and Response Set

Prompt-Level Decision Rule. For each prompt x , let define the returned response $\tilde{y} = y_{i^*}$ as the most representative member of dominant cluster k^* , i.e., cluster with largest total assignment mass. We use the inflated uncertainty $\hat{u}(x) \in \mathbb{R}^{[0,1]}$ as a prompt-level score so that small $\hat{u}(x)$ indicates robust semantic agreement after inflation, while large $\hat{u}(x)$ indicates cluster brittleness. Since CP requires one label per prompt, we define a prompt-level error label by evaluating the returned response $E(x) = e(x, \tilde{y}) \in \{0, 1\}$ where $E(x) = 0$ indicates that the returned response is correct. Using $\mathcal{I}_0 = \{\hat{u}(x) : x \in \mathcal{D}_{\text{cal}} \wedge E(x) = 0\}$ as calibration prompts whose returned response is correct, we calibrate a prompt acceptance threshold $\hat{\tau} = \text{Quantile}_{1-\alpha}(\mathcal{I}_0)$ which is $(1 - \alpha)$ -quantile

of scores $\hat{u}(\cdot)$ in the multiset \mathcal{I}_0 (if $\mathcal{I}_0 = \emptyset$, we abstain on all prompts). At inference, to answer a prompt x , we

$$\text{accept } x \iff \hat{u}(x) \leq \hat{\tau}; \quad \text{abstain otherwise.} \quad (18)$$

This calibration is appropriate since it aligns the prompt-level score $\hat{u}(x)$ with the prompt-level LLM outcome, i.e., correctness of the actually returned response \tilde{y} .

Theorem 1 (Conformal coverage for prompt acceptance). *Assume \tilde{y} and $\hat{u}(\cdot)$ are computed by the same procedure for calibration and test prompts under exchangeability of \mathcal{D}_{cal} and test prompt x_{new} . With the $(1 - \alpha)$ -quantile $\hat{\tau}$ defined on \hat{u} -space of prompts with correct returned responses, we have*

$$\mathbb{P}(\hat{u}(x_{\text{new}}) \leq \hat{\tau} \mid E(x_{\text{new}}) = 0) \geq 1 - \alpha. \quad (19)$$

Response-Level Prediction Sets. To construct CP-consistent prediction sets over sampled responses, we define a response-level non-conformity score that combines prompt uncertainty with response atypicality. Using the clustering outputs, we first define a response conformity measure

$$\phi_i = s_{i\hat{k}} \cdot \mathcal{P}(C_{\hat{k}}) \in \mathbb{R}^{[0,1]} \quad \text{s.t.} \quad \hat{k} = \arg \max_k s_{ik}, \quad (20)$$

which is large when response y_i is both strongly assigned to its best-matching semantic cluster and that cluster is well supported across samples. We then define the response-level non-conformity score (smaller is better) as,

$$S(x, y_i) = \frac{1}{2} \left(\hat{u}(x) + (1 - \phi_i) \right) \in \mathbb{R}^{[0,1]}, \quad (21)$$

which increases with prompt-level uncertainty $\hat{u}(x)$ and with response atypicality. Thus, a response attains a low score only when it arises from a low-uncertainty prompt and is semantically representative within a well-supported cluster. For calibration prompt-response pairs, we compute $S(x_j, y_{ji})$ in (21) and form the multiset $\mathcal{S}_0 = \{S(x_j, y_{ji}) : e_{ji} = 0\}$ of scores corresponding to correct responses. The $(1 - \alpha)$ -quantile threshold is then defined as $\hat{q} = \text{Quantile}_{1-\alpha}(\mathcal{S}_0)$. For a test prompt x with sampled responses $\mathcal{Y}(x) = \{y_i\}_{i=1}^n$, the response-level prediction set is

$$\mathcal{C}_{\alpha}(x) = \{y_i \in \mathcal{Y}(x) : S(x, y_i) \leq \hat{q}\}, \quad (22)$$

where the size of $\mathcal{C}_{\alpha}(x)$ provides a direct measure of response-level uncertainty. If a single output is required, we return the most representative response $\tilde{y} \in \mathcal{C}_{\alpha}(x)$.

Theorem 2 (Conformal coverage for prediction response sets). *Assume $S(x, y)$ is computed identically on calibration and test triples (x, y, e) under exchangeability with the same response sampling procedure. Considering \mathcal{C}_{α} defined in (22), for a randomly drawn test triple $(x_{\text{new}}, y_{\text{new}}, e_{\text{new}})$,*

$$\mathbb{P}(y_{\text{new}} \in \mathcal{C}_{\alpha}(x_{\text{new}}) \mid e_{\text{new}} = 0) \geq 1 - \alpha. \quad (23)$$

The proofs of the theorems and computational overhead analysis of our approach are reported in Appendices A and B, respectively.

4 Experimental Evaluations

We evaluate the performance of ACSE using discriminative and conformal analyses, benchmarking its ability to identify hallucinations (incorrect responses) reliably through adaptive uncertainty inflation against both uncalibrated and calibrated baselines. Appendix C describes the experimental setup and evaluation metrics.

Method	TriviaQA					CoQA					NQ					TruthfulQA					MMLU				
	AUROC	FPR@95	FPR@90	AUPR	AUARC	AUROC	FPR@95	FPR@90	AUPR	AUARC	AUROC	FPR@95	FPR@90	AUPR	AUARC	AUROC	FPR@95	FPR@90	AUPR	AUARC	AUROC	FPR@95	FPR@90	AUPR	AUARC
TE	0.65	0.78	0.72	0.63	0.61	0.60	0.85	0.79	0.54	0.58	0.62	0.82	0.75	0.57	0.60	0.55	0.88	0.81	0.50	0.53	0.52	0.90	0.84	0.50	0.52
P(True)	0.70	0.72	0.65	0.68	0.65	0.66	0.75	0.68	0.63	0.62	0.67	0.74	0.66	0.64	0.64	0.60	0.79	0.71	0.55	0.59	0.58	0.85	0.78	0.54	0.55
EigV	0.71	0.65	0.58	0.69	0.69	0.73	0.68	0.61	0.67	0.66	0.74	0.66	0.59	0.70	0.69	0.70	0.72	0.64	0.66	0.64	0.68	0.75	0.68	0.64	0.62
SU	0.73	0.55	0.49	0.73	0.72	0.74	0.60	0.53	0.71	0.70	0.75	0.58	0.50	0.72	0.73	0.71	0.65	0.57	0.68	0.68	0.69	0.69	0.61	0.65	0.65
DDCRP-CP	0.77	0.52	0.46	0.76	0.74	0.77	0.55	0.48	0.74	0.72	0.78	0.54	0.46	0.75	0.75	0.74	0.61	0.53	0.71	0.70	0.71	0.66	0.58	0.68	0.67
CAP	0.80	0.48	0.41	0.79	0.76	0.79	0.52	0.44	0.77	0.75	0.80	0.50	0.42	0.78	0.77	0.76	0.58	0.50	0.73	0.72	0.73	0.62	0.54	0.70	0.69
ACSE (Ours)	0.88	0.31	0.28	0.86	0.85	0.87	0.37	0.32	0.84	0.83	0.84	0.36	0.29	0.81	0.87	0.82	0.43	0.36	0.77	0.76	0.80	0.46	0.39	0.73	0.72

Table 1: Hallucination detection performance across diverse benchmarks using Mistral-7b. Metrics evaluate discrimination (AUROC \uparrow , AUPR \uparrow), safety (FPR@95 \downarrow , FPR@90 \downarrow), and selective generation (AUARC \uparrow).

Method	Mistral-7B					LLaMA-2-7B					Falcon-7B					Qwen-7B				
	AUROC	FPR@95	FPR@90	AUPR	AUARC	AUROC	FPR@95	FPR@90	AUPR	AUARC	AUROC	FPR@95	FPR@90	AUPR	AUARC	AUROC	FPR@95	FPR@90	AUPR	AUARC
TE	0.65	0.78	0.72	0.63	0.61	0.59	0.85	0.78	0.56	0.55	0.55	0.89	0.82	0.53	0.52	0.64	0.80	0.72	0.61	0.62
P(True)	0.70	0.72	0.65	0.68	0.65	0.65	0.77	0.69	0.61	0.61	0.61	0.81	0.74	0.58	0.59	0.70	0.72	0.65	0.67	0.68
EigV	0.71	0.65	0.58	0.69	0.69	0.69	0.66	0.59	0.66	0.67	0.67	0.72	0.64	0.62	0.64	0.74	0.61	0.54	0.71	0.72
SU	0.73	0.55	0.49	0.73	0.72	0.75	0.56	0.49	0.72	0.72	0.72	0.60	0.53	0.70	0.68	0.79	0.50	0.43	0.77	0.78
DDCRP-CP	0.77	0.52	0.46	0.76	0.74	0.77	0.52	0.45	0.74	0.74	0.74	0.57	0.49	0.71	0.72	0.82	0.47	0.40	0.79	0.81
CAP	0.80	0.48	0.41	0.79	0.76	0.79	0.48	0.41	0.76	0.76	0.76	0.54	0.46	0.73	0.74	0.84	0.43	0.36	0.81	0.83
ACSE (Ours)	0.89	0.28	0.24	0.88	0.87	0.86	0.35	0.29	0.83	0.84	0.84	0.38	0.32	0.81	0.82	0.91	0.25	0.19	0.89	0.90

Table 2: Hallucination detection performance on TriviaQA across diverse architectures. Metrics evaluate discrimination (AUROC \uparrow , AUPR \uparrow), safety (FPR@95 \downarrow , FPR@90 \downarrow), and selective generation (AUARC \uparrow).

Implementation Details. For each prompt, we generate $n = 10$ responses via nucleus sampling ($\eta = 0.9$) with temperature 0.3 to balance diversity and coherence and embed them using the sentence encoder all-MiniLM-L6. We perform HAC clustering with average linkage and cosine distance threshold $\epsilon = 0.35$. We set λ to equally weigh all brittleness features as $\mathbf{w} = \langle \frac{1}{5}, \frac{1}{5}, \frac{1}{5}, \frac{1}{5}, \frac{1}{5} \rangle$ to avoid any prioritization, and set the overconfidence penalty threshold τ_{ref} to the 75th percentile of the calibration base-uncertainty distribution. Each dataset uses 2000 samples split into disjoint calibration set (60%) and test set (40%). For Size-Stratified Coverage Violation (SSCV) evaluation, we define prediction set size strata as [1-2, 3-5, 6-7, 8-10]. The source codes are available at <https://github.com/tailabTMU/ACSE>.

Datasets. We evaluate on five benchmarks spanning open-domain retrieval, conversational QA, hallucination detection, and multi-domain reasoning: *TriviaQA* [Joshi *et al.*, 2017], *CoQA* [Reddy *et al.*, 2019], *Natural Questions (NQ)* [Kwiatkowski *et al.*, 2019], *TruthfulQA* [Lin *et al.*, 2022], and a stratified subset of *MMLU* [Wang *et al.*, 2024].

LLM Models. We use *Mistral-7B-Instruct* [Jiang *et al.*, 2024] which combines Grouped-Query Attention (GQA) and Sliding Window Attention (SWA) for strong performance with efficient inference. To assess model-agnosticism, we additionally evaluate *Llama-2-7B-Chat* [Touvron *et al.*, 2023], *Falcon-7B-Instruct* (Multi-Query Attention; MQA), and *Qwen-7B-Chat* [Bai *et al.*, 2023].

Baselines. We compare ACSE against six uncertainty methods spanning lexical, semantic, geometric, and calibrated approaches: *Token Entropy (TE)* [Vaswani *et al.*, 2017], *P(True)* [Kadavath *et al.*, 2022], *Semantic Uncertainty (SU)* [Kuhn *et al.*, 2023], and *EigV* [Lin *et al.*, 2024]. We

also include two CP-based calibrated frameworks: *DDCRP-CP* [Kaur *et al.*, 2024] and *Conformal Abstention Policy (CAP)* [Tayebati *et al.*, 2025]; we emphasize comparisons among DDCRP-CP, CAP, and ACSE since they share a CP calibration protocol, enabling standardized evaluation.

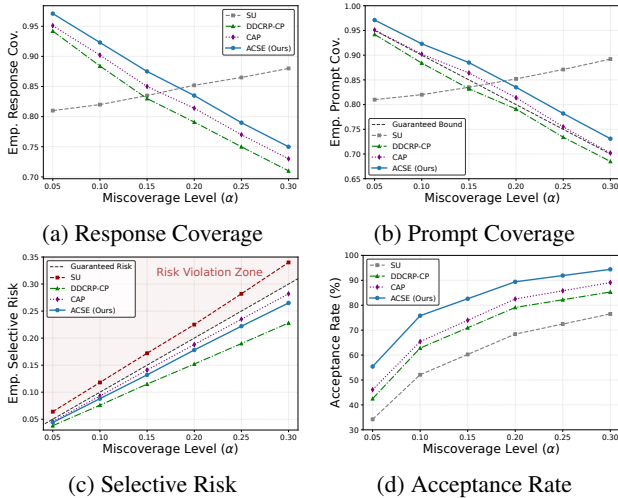
4.1 Results and Interpretations

We conduct an extensive empirical evaluation of ACSE to assess whether it (1) improves hallucination detection relative to state-of-the-art baselines, (2) strictly enforces user-specified coverage via conformal mechanisms along with the selective risk while maintaining high acceptance rates, and (3) improves uncertainty quantification on hallucinations against baselines.

Hallucination Detection Performance. This evaluation assesses the ACSE’s capability to distinguish between factually correct response generations and hallucinations across various datasets and LLMs. The results in Tables 1 and 2 demonstrate that ACSE achieves better discriminative performance across all benchmarks, e.g., on TriviaQA, ACSE increases AUROC to 0.88 from CAP’s 0.80. This improvement is particularly notable on high-efficiency models such as Falcon-7B where ACSE reduces 0.48 FPR@95 observed by CAP to 0.31, a 35.4% relative decrease in accepted hallucinations. Low standard deviations (0.01 to 0.02) across five independent runs confirm the statistical significance of the results. We report ablation studies and additional results on a text summarization dataset, recent 8B LLMs and baselines, together with base SE comparisons, probabilistic calibration results, and statistical significance tests in Appendix D.

Conformal Guarantees and Selective Risk. We assess ACSE reliability by varying α using both response-level and

Method	$\alpha = 0.05$ (Strict)						$\alpha = 0.10$ (Standard)						$\alpha = 0.20$ (Permissive)					
	Response-level			Prompt-level			Response-level			Prompt-level			Response-level			Prompt-level		
	R-Cov \uparrow	APS \downarrow	SSCV \downarrow	P-Cov \uparrow	Acc. \uparrow	Risk \downarrow	R-Cov \uparrow	APS \downarrow	SSCV \downarrow	P-Cov \uparrow	Acc. \uparrow	Risk \downarrow	R-Cov \uparrow	APS \downarrow	SSCV \downarrow	P-Cov \uparrow	Acc. \uparrow	Risk \downarrow
SU	0.823	1.05	0.081	0.810	34.2%	0.064	0.816	1.02	0.089	0.820	52.1%	0.118	0.808	1.01	0.115	0.852	68.4%	0.225
DDCRP-CP	0.941	1.95	0.046	0.942	42.5%	0.038	0.923	1.45	0.051	0.884	62.8%	0.076	0.810	1.22	0.074	0.791	79.1%	0.152
CAP	0.953	1.72	0.038	0.951	46.1%	0.046	0.902	1.32	0.042	0.917	65.4%	0.093	0.827	1.15	0.062	0.814	82.5%	0.188
ACSE (Ours)	0.985	1.32	0.024	0.971	55.4%	0.044	0.939	1.07	0.030	0.923	75.8%	0.088	0.842	1.08	0.045	0.835	89.4%	0.178

Table 3: Conformal analysis across varying α : Response Cov., APS, SSCV, Prompt Cov., Acceptance Rate (Acc.), and Selective Risk.Figure 2: Sensitivity analysis against varying miscoverage level α .

prompt-level metrics reported in Table 3, to enforce user-specified guarantees through conformal decision rules against baselines. Statistical reliability is reported through Response-level Coverage (R-Cov) which measures the inclusion rate of correct generated responses in the prediction sets, and Prompt-level Coverage (P-Cov) which evaluates the fraction of accepted prompts with correct returned responses. The analyses in Figure 2a show that ACSE guarantees superior R-Cov across all α levels. Similarly, Figure 2b demonstrates that ACSE consistently satisfies the theoretical prompt coverage guarantee, whereas baselines frequently exhibit undercoverage violations. ACSE also maintains low Average Prediction Set Size (APS) of 1.07 compared to 1.32 APS of CAP at $\alpha = 0.10$.

Additionally, ACSE achieves the lowest SSCV scores across all settings, e.g., 0.030 vs. 0.042 for CAP at $\alpha = 0.10$, indicating superior calibration stability across varying prediction set sizes. ACSE also consistently maximizes the Acceptance Rate (Acc.) across benchmarks, reaching 75.8% at $\alpha = 0.10$, a substantial improvement over the runner-up CAP at 65.4%. Furthermore, ACSE strictly guarantees the selective risk as the conditional error among accepted prompts that hallucinate, which is restricted by α as shown in Figure 2c. While the SU baseline suffers from overconfidence and risk violations, ACSE maintains a selective risk of 0.178 at low APS. ACSE also avoids the conservativeness of DDCRP-CP, which yields marginally lower risk but produces significantly larger prediction sets (1.45 vs. 1.07), trading precision for safety.

Uncertainty Quantification Analysis. This experiment evaluates the discriminative ability of our adjusted uncertainty score (\hat{u}) to separate correct responses from hallucinations.

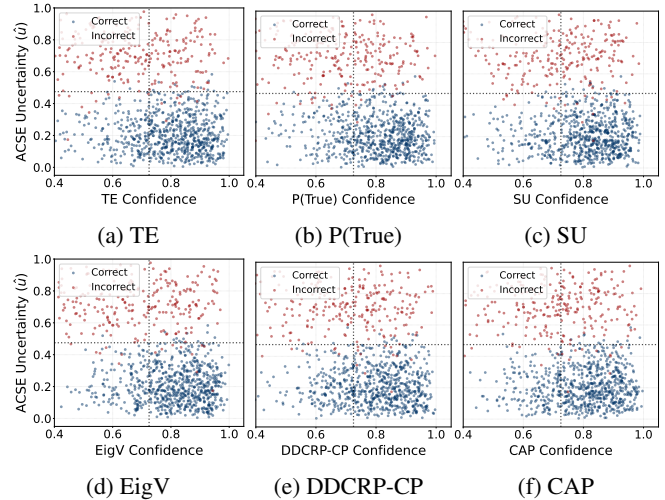


Figure 3: Comparing ACSE uncertainty against baseline confidences, distinguishing correct responses (blue) from hallucinations (red).

nations. Figure 3 illustrates this separation across four quadrants against each baseline. The top-left quadrant denotes the ideal abstention region for hallucinations where they exhibit both low baseline confidence and high ACSE uncertainty; conversely, the bottom-right quadrant denotes the ideal acceptance region for the correct responses. ACSE consistently assigns high uncertainty to hallucinations and low uncertainty to correct responses whereas the baselines exhibit varying ranges of confidence while hallucinating. The top-right quadrant highlights baseline failures compared to ACSE, in which hallucinations are incorrectly assigned high confidence but are correctly flagged by ACSE with high uncertainty.

5 Conclusion

We introduced ACSE to mitigate LLM overconfidence by quantifying uncertainty through semantic dispersion. Rather than treating uncertainty as a one-dimensional signal, ACSE employs an adaptive inflation mechanism to penalize semantic brittleness, ensuring reliable estimates. Evaluations across diverse benchmarks demonstrate that ACSE significantly improves hallucination detection, discriminative performance, and coverage guarantees. ACSE offers a robust solution for the reliable deployment of LLMs in safety-critical domains. Future work will explore adaptive sampling strategies to reduce computational overhead and extend the framework to conformal risk control for fine-grained quality calibration.

Acknowledgments

This research was undertaken thanks in part to funding from the Canada First Research Excellence Fund at Toronto Metropolitan University and Natural Sciences and Engineering Research Council of Canada (NSERC) Discovery grants (#348100).

References

- [Angelopoulos and Bates, 2023] Anastasios N Angelopoulos and Stephen Bates. Conformal prediction: A gentle introduction. *Foundations and Trends in Machine Learning*, 16(4):494–591, 2023.
- [Bai et al., 2023] Jinze Bai, Shuai Bai, Yunfei Chu, Zeyu Cui, Kai Dang, Xiaodong Deng, Yang Fan, Wenbin Ge, Yu Han, Fei Huang, et al. Qwen technical report. *arXiv preprint arXiv:2309.16609*, 2023.
- [Bhattacharjya et al., 2025] Debarun Bhattacharjya, Balaji Ganesan, Junkyu Lee, Radu Marinescu, Katsiaryna Mirylenka, Michael Glass, and Xiao Shou. Simba uq: Similarity-based aggregation for uncertainty quantification in large language models. *arXiv preprint arXiv:2510.13836*, 2025.
- [Brown et al., 2020] Tom Brown, Benjamin Mann, Nick Ryder, Melanie Subbiah, Jared D Kaplan, Prafulla Dhariwal, Arvind Neelakantan, Pranav Shyam, Girish Sastry, Amanda Askell, et al. Language models are few-shot learners. *Advances in neural information processing systems*, 33:1877–1901, 2020.
- [Cer et al., 2018] Daniel Cer, Yinfei Yang, Sheng-yi Kong, Nan Hua, Nicole Limtiaco, Rhomni St John, Noah Constant, Mario Guajardo-Cespedes, Steve Yuan, Chris Tar, et al. Universal sentence encoder. *arXiv preprint arXiv:1803.11175*, 2018.
- [Chang et al., 2024] Yupeng Chang, Xu Wang, Jindong Wang, Yuan Wu, Linyi Yang, Kaijie Zhu, Hao Chen, Xiaoyuan Yi, Cunxiang Wang, Yidong Wang, et al. A survey on evaluation of large language models. *ACM transactions on intelligent systems and technology*, 15(3):1–45, 2024.
- [Duan et al., 2023] Jinhao Duan, Hao Cheng, Shiqi Wang, Alex Zavalny, Chenan Wang, Renjing Xu, Bhavya Kailkhura, and Kaidi Xu. Shifting attention to relevance: Towards the predictive uncertainty quantification of free-form large language models. *arXiv preprint arXiv:2307.01379*, 2023.
- [Duan et al., 2024] Jinhao Duan, Hao Cheng, Shiqi Wang, Alex Zavalny, Chenan Wang, Renjing Xu, Bhavya Kailkhura, and Kaidi Xu. Shifting attention to relevance: Towards the predictive uncertainty quantification of free-form large language models. In *Proceedings of the 62nd Annual Meeting of the Association for Computational Linguistics*, volume 1, pages 5050–5063, 2024.
- [Fadeeva et al., 2024] Ekaterina Fadeeva, Aleksandr Rubashevskii, Artem Shelmanov, Sergey Petrakov, Haonan Li, Hamdy Mubarak, Evgenii Tsymbalov, Gleb Kuzmin, Alexander Panchenko, Timothy Baldwin, et al. Fact-checking the output of large language models via token-level uncertainty quantification. In *Findings of the Association for Computational Linguistics: ACL 2024*, pages 9367–9385, 2024.
- [Gao et al., 2021] Tianyu Gao, Xingcheng Yao, and Danqi Chen. Simcse: Simple contrastive learning of sentence embeddings. *arXiv preprint arXiv:2104.08821*, 2021.
- [Gliwa et al., 2019] Bogdan Gliwa, Iwona Mochol, Maciej Biesek, and Aleksander Wawer. Samsun corpus: A human-annotated dialogue dataset for abstractive summarization. In *Proceedings of the 2nd Workshop on New Frontiers in Summarization*, pages 70–79, 2019.
- [Granite Team, 2024] IBM Granite Team. Granite 3.0 language models. URL: <https://github.com/ibm-granite/granite-3.0-language-models>, 2024.
- [Guo et al., 2017] Chuan Guo, Geoff Pleiss, Yu Sun, and Kilian Q. Weinberger. On calibration of modern neural networks. In *Proceedings of the 34th International Conference on Machine Learning (ICML '17)*, volume 70 of *Proceedings of Machine Learning Research*, pages 1321–1330. PMLR, 2017.
- [Holtzman et al., 2020] Ari Holtzman, Jan Buys, Li Du, Maxwell Forbes, and Yejin Choi. The curious case of neural text degeneration. In *International Conference on Learning Representations (ICLR)*, 2020.
- [Huang et al., 2023] Yuheng Huang, Jiayang Song, Zhijie Wang, Shengming Zhao, Huaming Chen, Felix Juefei-Xu, and Lei Ma. Look before you leap: An exploratory study of uncertainty measurement for large language models. *arXiv preprint arXiv:2307.10236*, 2023.
- [Jiang et al., 2024] AQ Jiang, A Sablayrolles, A Mensch, C Bamford, DS Chaplot, Ddl Casas, F Bressand, G Lengyel, G Lample, L Saulnier, et al. Mistral 7b. *arXiv preprint arXiv:2310.06825*, 2024.
- [Joshi et al., 2017] Mandar Joshi, Eunsol Choi, Daniel S Weld, and Luke Zettlemoyer. TriviaQA: A large scale distantly supervised challenge dataset for reading comprehension. In *Proceedings of the 55th Annual Meeting of the Association for Computational Linguistics*, volume 1, pages 1601–1611, 2017.
- [Kadavath et al., 2022] Saurav Kadavath, Tom Conerly, Amanda Askell, Tom Henighan, Dawn Drain, Ethan Perez, Nicholas Schiefer, Zac Hatfield-Dodds, Nova DasSarma, Eli Tran-Johnson, et al. Language models (mostly) know what they know. *arXiv preprint arXiv:2207.05221*, 2022.
- [Kassianik et al., 2025] Paul Kassianik, Baturay Saglam, Alexander Chen, Blaine Nelson, Anu Vellore, Massimo Auffero, Fraser Burch, Dhruv Kedia, Avi Zohary, Sajana Weerawardhena, et al. Llama-3.1-foundationAI-securityLLM-base-8b technical report. *arXiv preprint arXiv:2504.21039*, 2025.
- [Kaur et al., 2024] Ramneet Kaur, Colin Samplawski, Adam D. Cobb, Anirban Roy, Brian Matejek, Manoj Acharya, Daniel Elenius, Alexander M. Berenbeim, John A.

- Pavlik, Nathaniel D. Bastian, and Susmit Jha. Addressing uncertainty in LLMs to enhance reliability in generative AI, 2024.
- [Kuhn *et al.*, 2023] Lorenz Kuhn, Yarin Gal, and Sebastian Farquhar. Semantic uncertainty: Linguistic invariances for uncertainty estimation in natural language generation. *arXiv preprint arXiv:2302.09664*, 2023.
- [Kwiatkowski *et al.*, 2019] Tom Kwiatkowski, Jennimaria Palomaki, Olivia Redfield, Michael Collins, Ankur Parikh, Chris Alberti, Danielle Epstein, Illia Polosukhin, Jacob Devlin, Kenton Lee, et al. Natural questions: a benchmark for question answering research. *Transactions of the Association for Computational Linguistics*, 7:453–466, 2019.
- [Lin *et al.*, 2022] Stephanie Lin, Jacob Hilton, and Owain Evans. TruthfulQA: Measuring how models mimic human falsehoods. In *Proceedings of the 60th annual meeting of the association for computational linguistics*, volume 1, pages 3214–3252, 2022.
- [Lin *et al.*, 2024] Zhen Lin, Shubhendu Trivedi, and Jimeng Sun. Generating with confidence: Uncertainty quantification for black-box large language models, 2024.
- [Liu *et al.*, 2023] Yiheng Liu, Tianle Han, Siyuan Ma, Jiayue Zhang, Yuanyuan Yang, Jiaming Tian, Hao He, Antong Li, Mengshen He, Zhengliang Liu, et al. Summary of chatgpt-related research and perspective towards the future of large language models. *Meta-radiology*, 1(2):100017, 2023.
- [Murtagh and Contreras, 2017] Fionn Murtagh and Pedro Contreras. Algorithms for hierarchical clustering: an overview, ii. *Wiley Interdisciplinary Reviews: Data Mining and Knowledge Discovery*, 7(6):e1219, 2017.
- [Nikitin *et al.*, 2024] Alexander Nikitin, Jannik Kossen, Yarin Gal, and Pekka Marttinen. Kernel language entropy: Fine-grained uncertainty quantification for LLMs from semantic similarities. *Advances in Neural Information Processing Systems*, 37:8901–8929, 2024.
- [Reddy *et al.*, 2019] Siva Reddy, Danqi Chen, and Christopher D Manning. CoQA: A conversational question answering challenge. *Transactions of the Association for Computational Linguistics*, 7:249–266, 2019.
- [Reimers and Gurevych, 2019] Nils Reimers and Iryna Gurevych. Sentence-bert: Sentence embeddings using siamese bert-networks. In *Conference on Empirical Methods in Natural Language Processing (EMNLP)*, 2019.
- [Shanahan, 2024] Murray Shanahan. Talking about large language models. *Communications of the ACM*, 67(2):68–79, 2024.
- [Shorinwa *et al.*, 2025] Ola Shorinwa, Zhiting Mei, Justin Lillard, Allen Z Ren, and Anirudha Majumdar. A survey on uncertainty quantification of large language models: Taxonomy, open research challenges, and future directions. *ACM Computing Surveys*, 2025.
- [Tayebati *et al.*, 2025] Sina Tayebati, Divake Kumar, Nataran Darabi, Dinithi Jayasuriya, Ranganath Krishnan, and Amit Ranjan Trivedi. Learning conformal abstention policies for adaptive risk management in large language and vision-language models. *arXiv preprint arXiv:2502.06884*, 2025.
- [Teubner *et al.*, 2023] Timm Teubner, Christoph M Flath, Christof Weinhardt, Wil Van Der Aalst, and Oliver Hinz. Welcome to the era of chatgpt et al. the prospects of large language models. *Business & Information Systems Engineering*, 65(2):95–101, 2023.
- [Thirunavukarasu *et al.*, 2023] Arun James Thirunavukarasu, Darren Shu Jeng Ting, Kabilan Elangovan, Laura Gutierrez, Ting Fang Tan, and Daniel Shu Wei Ting. Large language models in medicine. *Nature medicine*, 29(8):1930–1940, 2023.
- [Touvron *et al.*, 2023] Hugo Touvron, Louis Martin, Kevin Stone, Peter Albert, Amjad Almahairi, Yasmine Babaei, Nikolay Bashlykov, Soumya Batra, Prajjwal Bhargava, Shruti Bhosale, et al. Llama 2: Open foundation and fine-tuned chat models. *arXiv preprint arXiv:2307.09288*, 2023.
- [Vaswani *et al.*, 2017] Ashish Vaswani, Noam Shazeer, Niki Parmar, Jakob Uszkoreit, Llion Jones, Aidan N Gomez, Łukasz Kaiser, and Illia Polosukhin. Attention is all you need. *Advances in neural information processing systems*, 30, 2017.
- [Vovk *et al.*, 2005] Vladimir Vovk, Alexander Gammerman, and Glenn Shafer. *Algorithmic learning in a random world*. Springer, 2005.
- [Wang *et al.*, 2024] Yubo Wang, Xueguang Ma, Ge Zhang, Yuansheng Ni, Abhranil Chandra, Shiguang Guo, Weiming Ren, Aaran Arulraj, Xuan He, Ziyang Jiang, et al. Mmlu-pro: A more robust and challenging multi-task language understanding benchmark. *Advances in Neural Information Processing Systems*, 37:95266–95290, 2024.
- [Yadkori *et al.*, 2024] Yasin Abbasi Yadkori, Ilja Kuzborskij, András György, and Csaba Szepesvári. To believe or not to believe your LLM. *arXiv preprint arXiv:2406.02543*, 2024.
- [Yao *et al.*, 2019] Jiayu Yao, Weiwei Pan, Soumya Ghosh, and Finale Doshi-Velez. Quality of uncertainty quantification for bayesian neural network inference. *arXiv preprint arXiv:1906.09686*, 2019.
- [Yarie *et al.*, 2024] Liz Yarie, Dominic Soriano, Leonard Kaczmarek, Benjamin Wilkinson, and Eduardo Vasquez. Mitigating token-level uncertainty in retrieval-augmented large language models. *Authorea Preprints*, 2024.
- [Zheng *et al.*, 2026] Xingyu Zheng, Yuye Li, Haoran Chu, Yue Feng, Xudong Ma, Zining Wang, Jie Luo, Jinyang Guo, Haotong Qin, Michele Magno, et al. An empirical study of qwen3 quantization. *Visual Intelligence*, 4(1):11, 2026.

A Proofs

Proof of Theorem 1. We analyze the probability of acceptance conditional on the event that the returned response is correct, $E(x_{\text{new}}) = 0$. Let $\mathcal{I}_0 = \{\hat{u}(x) : x \in \mathcal{D}_{\text{cal}} \wedge E(x) = 0\}$ be the multiset of inflated uncertainty scores for the calibration prompts that resulted in correct responses, and let $M_0 = |\mathcal{I}_0|$. By the assumption of exchangeability between the calibration set \mathcal{D}_{cal} and the test prompt x_{new} , the score $\hat{u}(x_{\text{new}})$ is exchangeable with the elements of \mathcal{I}_0 conditional on $E(x_{\text{new}}) = 0$. Consequently, the rank of $\hat{u}(x_{\text{new}})$ among the $M_0 + 1$ scores in $\mathcal{I}_0 \cup \{\hat{u}(x_{\text{new}})\}$ is uniformly distributed on $\{1, \dots, M_0 + 1\}$. The threshold $\hat{\tau}$ is defined as the empirical $(1 - \alpha)$ -quantile of \mathcal{I}_0 . Following standard conformal prediction theory, this quantile is chosen such that it covers at least a fraction $1 - \alpha$ of the exchangeable distribution. Therefore,

$$\mathbb{P}(\hat{u}(x_{\text{new}}) \leq \hat{\tau} \mid E(x_{\text{new}}) = 0) \geq 1 - \alpha. \quad (24)$$

□

Proof of Theorem 2. We analyze the probability of inclusion conditional on the event that the specific response is correct, $e_{\text{new}} = 0$. Let $\mathcal{S}_0 = \{S(x_j, y_{ji}) : e_{ji} = 0\}$ be the multiset of non-conformity scores for all correct responses in the calibration set. Due to the exchangeability of the calibration and test data triples (x, y, e) , the test score $S(x_{\text{new}}, y_{\text{new}})$ is exchangeable with the elements of \mathcal{S}_0 conditional on $e_{\text{new}} = 0$. The threshold \hat{q} is defined as the $(1 - \alpha)$ -quantile of \mathcal{S}_0 . By the standard conformal prediction guarantee, the probability that a new exchangeable score does not exceed this quantile is at least $1 - \alpha$. Since the prediction set is defined as $\mathcal{C}_\alpha(x_{\text{new}}) = \{y \in \mathcal{Y}(x_{\text{new}}) : S(x_{\text{new}}, y) \leq \hat{q}\}$, the condition $S(x_{\text{new}}, y_{\text{new}}) \leq \hat{q}$ is equivalent to $y_{\text{new}} \in \mathcal{C}_\alpha(x_{\text{new}})$. Therefore,

$$\mathbb{P}(y_{\text{new}} \in \mathcal{C}_\alpha(x_{\text{new}}) \mid e_{\text{new}} = 0) \geq 1 - \alpha. \quad (25)$$

□

B Computational Overhead Analysis

The dominant overhead comes from generating multiple responses per prompt. By contrast, the ACSE-specific semantic module is lightweight and depends only on the small bounded sampling budget n (in our experiments, $n = 10$). This additional cost is justified in safety-critical settings, where improved reliability and calibrated abstention are more important than maximizing raw throughput.

For a prompt x , ACSE samples n responses y_1, \dots, y_n . Let $C_{\text{gen}}(y_i)$ denote the cost of generating response y_i . We keep this term abstract, since its exact value depends on the base LLM, hardware, batching, and implementation. Let d be the embedding dimension and K the number of semantic clusters returned by HAC, where $1 < K \leq n$. The per-prompt runtime can be written as

$$\mathcal{T}(x) = \sum_{i=1}^n C_{\text{gen}}(y_i) + \mathcal{O}(n^2 d + n^2 \log n + nKd). \quad (26)$$

The three semantic terms in (26) correspond to (1) $\mathcal{O}(n^2 d)$ for pairwise cosine geometry over the n response embeddings

Method	Total Latency (s)	Relative Cost	Sampling Time (s)	Post-processing (s)	Peak Memory (GB)
One-shot decoding	0.86	1.0×	0.86	0.00	9.3
DDCRP-CP	4.89	5.7×	4.21	0.68	11.6
CAP	5.16	6.0×	4.21	0.95	12.0
ACSE (Ours)	5.47	6.4×	4.21	1.26	12.3

Table 4: Computational overhead (Llama-3-8B; TriviaQA).

in \mathbb{R}^d , (2) $\mathcal{O}(n^2 \log n)$ for average-linkage hierarchical agglomerative clustering, and (3) $\mathcal{O}(nKd)$ for centroid-based soft assignment and prompt-level semantic aggregation. Since $K \leq n$, the semantic post-processing depends only on the small response budget n and the embedding dimension d , not on the parameter count of the base LLM. Therefore, ACSE is not purely linear in n , but its practical bottleneck remains repeated response generation, not the semantic uncertainty computation itself. In particular, the inflation rule and final prompt-level feature computation are negligible once the responses have already been generated.

The same pipeline is used during calibration and deployment, but its impact differs across phases. During calibration, the cost is paid once offline to compute the conformal operating point. During deployment, the per-prompt latency is governed directly by (26). Thus, the main computational concern is online inference rather than offline calibration.

The ACSE-specific memory overhead comes from storing the semantic objects associated with the n sampled responses of one prompt: the response embeddings in \mathbb{R}^d , the pairwise similarity or distance matrix used by HAC, and the response-to-cluster soft assignments. Thus, the per-prompt memory overhead is

$$\mathcal{M}(x) = \mathcal{O}(nd + n^2 + nK) = \mathcal{O}(nd + n^2), \quad (27)$$

since $K \leq n$. Importantly, ACSE does not replicate the base LLM in memory; it only adds a small semantic buffer on top of standard model inference memory. For the bounded regime used in this work ($n = 10$), this overhead remains modest.

We measure the computational overhead of ACSE, DDCRP-CP, and CAP under the same hardware and decoding setup on TriviaQA using Llama-3-8B. In addition to end-to-end latency, we report a decomposition into shared sampling cost and method-specific post-processing cost, allowing us to separate the cost of uncertainty estimation from the cost of generating multiple responses, which is common to all multi-sample methods. As shown in Table 4, ACSE has the highest end-to-end latency among the compared methods, which is expected for a multi-sample semantic uncertainty approach. However, the dominant cost for all three conformal methods comes from shared response sampling rather than from method-specific processing. Relative to one-shot decoding, DDCRP-CP, CAP, and ACSE require 5.7×, 6.0×, and 6.4× total latency, respectively. The additional ACSE-specific post-processing overhead is limited, exceeding DDCRP-CP by only 0.58 s and CAP by 0.31 s. Peak memory follows the same trend, with ACSE remaining only slightly above the other multi-sample baselines. These results show that although ACSE is more expensive than simpler conformal methods, most of the overhead comes from shared multi-sample generation, while the extra cost of the adaptive semantic inflation step remains modest.

Method	TriviaQA					SamSum				
	AUROC	FPR@95	FPR@90	AUPR	AUARC	AUROC	FPR@95	FPR@90	AUPR	AUARC
SAR	.836 ± .005	.403 ± .011	.349 ± .010	.821 ± .006	.811 ± .006	.786 ± .006	.492 ± .012	.428 ± .011	.767 ± .007	.756 ± .007
KLE	.851 ± .004	.374 ± .010	.323 ± .009	.834 ± .005	.823 ± .005	.798 ± .005	.468 ± .011	.408 ± .010	.779 ± .006	.768 ± .006
SIMBA	.844 ± .005	.389 ± .010	.336 ± .009	.828 ± .006	.817 ± .006	.792 ± .006	.481 ± .011	.418 ± .010	.774 ± .006	.762 ± .006
ACSE (Ours)	.872 ± .004	.332 ± .009	.286 ± .008	.849 ± .005	.844 ± .005	.807 ± .005	.447 ± .010	.389 ± .009	.786 ± .006	.776 ± .006

Table 5: Task-agnostic discriminative performance on Llama-3-8B.

Method	Llama-3-8B					Qwen-3-8B					Granite-3.1-8B				
	AUROC	FPR@95	FPR@90	AUPR	AUARC	AUROC	FPR@95	FPR@90	AUPR	AUARC	AUROC	FPR@95	FPR@90	AUPR	AUARC
SAR	.836 ± .005	.403 ± .011	.349 ± .010	.821 ± .006	.811 ± .006	.833 ± .005	.410 ± .011	.355 ± .010	.818 ± .006	.808 ± .006	.826 ± .006	.421 ± .012	.365 ± .011	.810 ± .007	.800 ± .007
KLE	.851 ± .004	.374 ± .010	.323 ± .009	.834 ± .005	.823 ± .005	.848 ± .004	.381 ± .010	.329 ± .009	.830 ± .005	.819 ± .005	.841 ± .005	.392 ± .011	.339 ± .010	.823 ± .006	.812 ± .006
SIMBA	.844 ± .005	.389 ± .010	.336 ± .009	.828 ± .006	.817 ± .006	.840 ± .005	.397 ± .010	.343 ± .009	.824 ± .006	.813 ± .006	.834 ± .006	.407 ± .011	.351 ± .010	.817 ± .006	.806 ± .006
ACSE (Ours)	.872 ± .004	.332 ± .009	.286 ± .008	.849 ± .005	.844 ± .005	.869 ± .004	.338 ± .009	.291 ± .008	.846 ± .005	.842 ± .005	.863 ± .005	.349 ± .010	.301 ± .009	.839 ± .005	.836 ± .005

Table 6: Discriminative performance across additional models/methods on TriviaQA.

Method	TriviaQA		CoQA		NQ	
	AUROC	FPR@95	AUROC	FPR@95	AUROC	FPR@95
SE Score	0.77	0.49	0.75	0.55	0.76	0.52
ACSE (Inflated)	0.88	0.31	0.87	0.37	0.84	0.36
<i>Absolute Gain</i>	<i>+0.11</i>	<i>-0.18</i>	<i>+0.12</i>	<i>-0.18</i>	<i>+0.08</i>	<i>-0.16</i>

Table 7: Comparative analysis of ACSE against Base SE score.

Method	$\alpha = 0.05$ (Strict)		$\alpha = 0.10$ (Standard)		$\alpha = 0.20$ (Permissive)	
	ECE ↓	Brier ↓	ECE ↓	Brier ↓	ECE ↓	Brier ↓
SU	0.17	0.25	0.16	0.24	0.14	0.22
DDCRP-CP	0.10	0.15	0.09	0.14	0.07	0.12
CAP	0.07	0.12	0.06	0.11	0.05	0.10
ACSE (Ours)	0.06	0.10	0.04	0.09	0.03	0.08

Table 8: Probabilistic calibration analysis across varying α .

C Experimental Setup and Metrics

We implement all methods in PyTorch v2.1.2 and HuggingFace Transformers v4.40.0, using sentence-transformers to embed generated responses. For valid comparison, the uncalibrated SU baseline is post-hoc calibrated with isotonic regression to map raw scores to observed error frequencies. We use Llama-3-8B as our primary model on TriviaQA as our primary dataset by default. All experiments were run on an AMD Ryzen 9 5900X (12-core) workstation with a single NVIDIA RTX 3060 GPU (16GB VRAM).

C.1 Evaluation Metrics

Let $\{(x, y)_i \mid x \in \mathcal{D}_{\text{val}}, y \in \mathcal{Y}(x)\}_{i=1}^N$ be the set of validation prompt-response pairs, $\hat{u}(x)$ be an uncertainty score, and accept (answer) each prompt when $\hat{u}(x) \leq \hat{\tau}$. We compute the *acceptance rate* as,

$$\text{AccRate}(\hat{\tau}) = \frac{1}{N} \sum_{i=1}^N \mathbb{1}\{\hat{u}(x_i) \leq \hat{\tau}\}. \quad (28)$$

To avoid ambiguity, we distinguish *conformal set coverage* (membership of the correct response in a prediction set) from *acceptance rate*, i.e., the fraction of prompts on which ACSE returns an answer rather than abstaining.

The empirical selective risk is also defined as conditional error among accepted prompts, indicating the fraction of accepted prompts whose returned responses are incorrect

Dataset	ACSE vs. KLE			ACSE vs. SAR			ACSE vs. SIMBA		
	AUROC	FPR@95	AUARC	AUROC	FPR@95	AUARC	AUROC	FPR@95	AUARC
TriviaQA	0.004	0.002	0.006	0.001	0.001	0.002	0.002	0.001	0.004
SamSum	0.018	0.015	0.021	0.006	0.004	0.009	0.011	0.009	0.016

Table 9: Paired significance tests (p -values) for Table 5.

(hallucinating accepted prompts) with binary error labels $\{E_i = e(x, \hat{y})\}_{i=1}^N$ of returned responses \hat{y} , and computed as,

$$\hat{R}(\hat{\tau}) = \frac{\sum_{i=1}^N E_i \mathbb{1}\{\hat{u}(x_i) \leq \hat{\tau}\}}{\sum_{i=1}^N \mathbb{1}\{\hat{u}(x_i) \leq \hat{\tau}\}}. \quad (29)$$

For computing AUARC (Area under the Accuracy-Rejection curve), we calculate the accuracy among accepted prompts as,

$$\text{Acc}(\hat{\tau}) = \frac{\sum_{i=1}^N (1 - E_i) \mathbb{1}\{\hat{u}(x_i) \leq \hat{\tau}\}}{\sum_{i=1}^N \mathbb{1}\{\hat{u}(x_i) \leq \hat{\tau}\}}, \quad (30)$$

which measures the rate of the accepted prompts that have correct returned response. The rejection rate is computed as,

$$\text{Rej}(\hat{\tau}) = \frac{1}{N} \sum_{i=1}^N \mathbb{1}\{\hat{u}(x_i) > \hat{\tau}\}. \quad (31)$$

For prediction set $\mathcal{C}_\alpha(\cdot)$, the empirical CP coverage (prediction response set coverage) is computed as,

$$\text{R-Cov}_{1-\alpha} = \frac{\sum_{i=1}^N \mathbb{1}\{e_i = 0\} \mathbb{1}\{y_i \in \mathcal{C}_\alpha(x_i)\}}{\sum_{i=1}^N \mathbb{1}\{e_i = 0\}} \quad (32)$$

$$= \frac{1}{N_0^R} \sum_{(j,i): e_{ji}=0} \mathbb{1}\{y_{ji} \in \mathcal{C}_\alpha(x_j)\}, \quad (33)$$

where $N_0^R = |\{(j, i) \in \mathcal{D}_{\text{test}} : e_{ji} = 0\}|$ as the size of prompt-response pairs in the test set whose responses are correct. The prompt-level coverage computes the fraction of test prompts with correct returned responses that are successfully

accepted by the calibrated threshold, and is defined as,

$$\begin{aligned} \text{P-Cov}_{1-\alpha} &= \frac{\sum_{i=1}^N \mathbb{1}\{E_i = 0\} \mathbb{1}\{\hat{u}(x_i) \leq \hat{\tau}\}}{\sum_{i=1}^N \mathbb{1}\{E_i = 0\}} \\ &= \frac{1}{N_0^P} \sum_{i: E_i=0} \mathbb{1}\{\hat{u}(x_i) \leq \hat{\tau}\}, \end{aligned} \quad (34)$$

where $N_0^P = |\{i \in \mathcal{D}_{\text{test}} : E_i = 0\}|$ as the size of set of prompts in the test set whose returned responses are correct. It empirically verifies whether our method meets the theoretical guarantee of covering the accepted prompts with correct returned responses with a probability of at least $1 - \alpha$. Then, the average prediction set size (APS) is computed as,

$$\text{APS} = \frac{1}{N} \sum_{i=1}^N |\mathcal{C}_\alpha(x_i)|. \quad (36)$$

To compute SSCV (Size-Stratified Coverage Violation), let $|\mathcal{C}_\alpha(x_i)|$ be the prediction set size for each prompt and partition the test prompts into B disjoint strata $\{\mathcal{G}_b\}_{b=1}^B$ by fixed ranges of their prediction set size. We report SSCV as the worst-case shortfall across coverage strata $\text{Cov}_b = 1/|\mathcal{G}_b| \sum_{i \in \mathcal{G}_b} \mathbb{1}\{y_i \in \mathcal{C}_\alpha(x_i)\}$ as,

$$\text{SSCV} = \max_{b \in [B]} \left((1 - \alpha) - \text{Cov}_b \right)_+,$$

where $(\cdot)_+ = \max\{\cdot, 0\}$ and Cov_b is the stratum-wise empirical coverage.

D Additional Experimental Results

Datasets. We additionally evaluate on SamSum [Gliwa *et al.*, 2019] to include human-written dialogues paired with abstractive summaries, which enables evaluation of conversational summarization quality.

LLM Models. In addition to the 7B-parameter models, we evaluate three 8B-parameter models: Llama-3-8B [Kassianik *et al.*, 2025], Qwen-3-8B [Zheng *et al.*, 2026], and Granite-3.1-8B [Granite Team, 2024].

Baselines. We further compare ACSE against SAR [Duan *et al.*, 2024], KLE [Nikitin *et al.*, 2024], and SIMBA [Bhattacharjya *et al.*, 2025], alongside the baselines used in the main experiments.

Discriminative Performance across Models and Tasks. To strengthen timeliness and generalizability, we extend our evaluation beyond QA tasks to include the summarization benchmark SamSum where ACSE consistently outperforms all baselines on the corresponding discriminative metrics. We further conduct same-protocol experiments using more recent models including Llama-3-8B, Qwen-3-8B, and Granite-3.1-8B, against additional baselines such as KLE, SAR, and SIMBA. SAR estimates uncertainty through relevance-weighted semantic consistency across generated responses. On the other hand, KLE captures fine-grained uncertainty using kernel-based semantic similarity distributions while SIMBA improves similarity aggregation. ACSE, in contrast, further addresses cluster

brittleness and conformalizes the adjusted uncertainty score to provide finite-sample guarantees. As shown in Table 5, ACSE remains the strongest method across both datasets. Gains are observed on SamSum, where ACSE improves AUROC to 0.807 and consistently lowers FPR@95 to 0.447 over all baselines. As shown in Table 6, ACSE remains the strongest method across all three architectures, achieving consistent improvements over KLE on TriviaQA, e.g., AUROC 0.872 (Llama-3-8B), 0.869 (Qwen-3-8B), and 0.863 (Granite-3.1-8B), along with corresponding reductions in FPR@95.

Base SE vs. ACSE Performance Analysis. This ablation isolates the performance contribution of the adaptive inflation mechanism by benchmarking base Semantic Entropy (SE) against ACSE across three datasets. As shown in Table 7, adaptive inflation is the primary driver of improved error detection, yielding significant absolute AUROC increases up to +0.12 on CoQA, and a substantial reduction in FPR@95 across all benchmarks. Most notably, the inflation mechanism identifies overconfident errors missed by uninflated signals, reducing the FPR@95 by 0.18 on TriviaQA and CoQA. This gap confirms that raw entropy scores often fails to detect unstable semantic clusters; by leveraging semantic features to inflate uncertainty values for brittle responses, ACSE successfully prevents incorrect answers from passing the conformal threshold.

Probabilistic Model Calibration. This evaluation assesses how well uncertainty scores reflect the actual likelihood of correctness using Expected Calibration Error (ECE) [Guo *et al.*, 2017] and Brier Score. As shown in Table 8, ACSE significantly outperforms all baselines across all miscalibration levels. For example, ACSE reduces ECE to 0.03 in the permissive region, a nearly fivefold improvement the overconfident SU baseline. This performance extends to Brier scores, which ACSE consistently maintains below 0.10, confirming that semantic-level inflation provides a robust confidence signal regardless of the specified tolerance.

Statistical Significance Analysis. To complement the mean \pm std results, we additionally perform paired significance tests on the main baseline comparison. Since all methods are evaluated on the same prompts, we use paired bootstrap tests over prompts for the primary metrics: AUROC, FPR@95, and AUARC. This allows us to verify that the gains of ACSE over the strongest recent baselines are not explained by run-to-run variation alone. Paired statistical significance results for Table 5 are shown in Table 9. Using a paired bootstrap test over prompts, the gains of ACSE over the strongest baselines remain statistically significant on the main metrics. On TriviaQA, improvements over both KLE and SIMBA are significant across AUROC, FPR@95, and AUARC, with all $p < 0.01$. On SamSum, the gains are smaller but remain significant, with all $p < 0.02$. These results strengthen the conclusion that the improvements of ACSE are not explained by run-to-run variation alone.

D.1 Ablation Studies

We conduct comprehensive ablation studies to examine ACSE’s performance, covering brittleness feature contributions, clustering threshold and sampling size sensitivities,

Region	Threshold (ϵ)	AUROC	Impact Explanation
Over-Fragmentation	0.10	0.72	Splits paraphrases (High False Positives) Fragments minor lexical variations
	0.20	0.78	
Optimal	0.35	0.83	Correctly groups semantic equivalents
Under-Fragmentation	0.50	0.75	Merges distinct but close meanings Merges contradictions (Masks Uncertainty)
	0.70	0.65	

Table 10: Sensitivity Analysis of the clustering threshold ϵ .

Configuration	TriviaQA		CoQA	
	AUROC	FPR@95	AUROC	FPR@95
Full ACSE Framework	0.88	0.31	0.87	0.37
w/o Cluster Size Penalty	0.87	0.32	0.86	0.38
w/o Margin-to-threshold	0.87	0.33	0.86	0.39
w/o Cluster Dispersion	0.86	0.34	0.85	0.40
w/o Centroid Distance	0.85	0.35	0.84	0.42
w/o Cluster-membership Entropy	0.82	0.438	0.81	0.45

Table 11: Cluster robustness feature ablation analysis.

calibration size behavior, and robustness to implementation choices such as weighting schemes and sentence encoders.

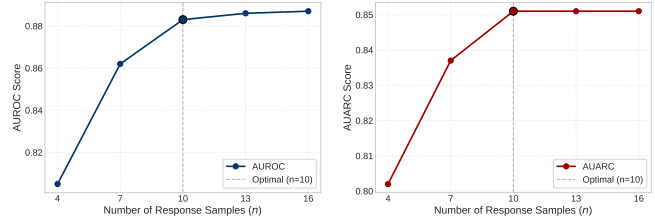
Sensitivity to Clustering Threshold. This experiment evaluates the robustness of ACSE to the semantic clustering threshold ϵ , which controls cluster resolution by setting the minimum similarity required to group responses. By varying ϵ from 0.10 to 0.70, we investigated the trade-off between over-fragmentation and under-fragmentation. As detailed in Table 10 and Figure 5a, the discriminative performance follows a clear bell-shaped curve that peaks at an optimal threshold of $\epsilon = 0.35$ with an AUROC of 0.83. While low thresholds ($\epsilon \leq 0.20$) are overly restrictive and high thresholds ($\epsilon \geq 0.50$) mask uncertainty by merging distinct meanings, the peak at 0.35 successfully captures linguistic invariances for robust uncertainty estimation.

Contribution of Cluster Brittleness Features. This study uses a leave-one-out ablation to quantify the contribution of each semantic feature within the inflation function λ towards discriminative performance. As shown in Table 11 and Figure 5b, Cluster-membership Entropy is the most critical feature; its removal results in 0.06 AUROC drop, confirming that mapping ambiguity is the strongest predictor of factual errors. Centroid Distance and Cluster Dispersion follow as secondary signals, indicating that the internal tightness of a cluster provides essential confidence information that raw entropy lacks. Conversely, the minimal impact of removing the Cluster Size Penalty suggests that the structural arrangement and stability of samples are more informative than their raw count. The results show the marginal effect of removing each feature from the full ACSE system that measures each feature’s contribution in the presence of the others, not its standalone importance or optimal weight, e.g., the larger drop from removing SE indicates it is the strongest signal, not that other features should be down-weighted.

Sample Size Sensitivity Analysis. This experiment evaluates the impact of response sample size (n) on the framework’s ability to distinguish between hallucinations and correct responses. By varying n from 4 to 16, we aimed to identify the elbow point where the increase in computational cost no longer yields significant performance gains. As shown in Ta-

No. of Response Samples	AUROC	AUARC
$n = 4$	0.805	0.802
$n = 7$	0.862	0.837
$n = 10$	0.883	0.851
$n = 13$	0.886	0.851
$n = 16$	0.887	0.851

Table 12: Sample Size versus ACSE Discriminative Performance.



(a) AUROC vs. Sample Size

(b) AUARC vs. Sample Size

Figure 4: Sensitivity analysis of the response sample size n .

ble 12 and Figure 4, discriminative performance significantly improves as the sample size increases from $n = 4$ to $n = 10$. However, beyond $n = 10$, both metrics plateau; AUARC remains constant at 0.851, and increases in AUROC become marginal. This confirms that 10 samples provide the optimal trade-off between semantic resolution and inference cost.

Calibration Size Sensitivity. The calibration set should satisfy exchangeability assumption (Section 3) which is less restrictive than being from the same distribution. To measure sensitivity to the calibration set size, we include an ablation study in Table 13 varying the calibration fraction from 10% to 40%. ACSE consistently provides the strongest overall tradeoff between coverage, compact prediction sets, acceptance, and selective risk across all calibration sizes. At 10% calibration, ACSE achieves higher prompt coverage than CAP and DDCRP-CP (0.904 vs. 0.889 and 0.872), together with the highest acceptance rate (72.8% vs. 70.2% and 68.1%). A similar trend is observed for discrimination and safety metrics. ACSE consistently outperforms both CAP and DDCRP-CP in AUROC, FPR@95, and AUARC across all calibration fractions. At 10% calibration, ACSE improves AUROC to 0.861, compared with 0.792 for CAP while reducing FPR@95 to 0.352 from 0.486 respectively. The same ordering remains at 20%–40%, with only gradual gains as the calibration pool increases. These results indicate that ACSE’s advantage is not an artifact of extensive calibration, but remains visible even under substantially smaller calibration budgets.

Weight Sensitivity of Brittleness Features. In the experiments, we use $\mathbf{w} = \langle \frac{1}{5}, \frac{1}{5}, \frac{1}{5}, \frac{1}{5}, \frac{1}{5} \rangle$ as a deliberate design choice (not as learned parameters fit to labels). Since all five brittleness components are normalized to $[0, 1]$, equal weights provide a fair and neutral choice without privileging any feature a priori. This does not imply that equal weighting is required; different deployments may reasonably emphasize different semantic risks (e.g., ambiguity vs. overconfidence vs. sparse support) by user-

Metric	DDCRP-CP				CAP				ACSE (Ours)				
	10%	20%	30%	40%	10%	20%	30%	40%	10%	20%	30%	40%	
Discr.	AUROC	.788 ± .007	.794 ± .007	.800 ± .006	.805 ± .006	.781 ± .008	.788 ± .007	.794 ± .007	.799 ± .006	.850 ± .005	.857 ± .005	.862 ± .005	.866 ± .004
	FPR@95	.482 ± .013	.473 ± .012	.466 ± .011	.460 ± .011	.497 ± .014	.486 ± .013	.476 ± .012	.469 ± .012	.366 ± .010	.357 ± .010	.351 ± .009	.346 ± .009
	AUARC	.728 ± .008	.734 ± .008	.739 ± .007	.743 ± .007	.722 ± .008	.729 ± .008	.734 ± .007	.739 ± .007	.824 ± .006	.828 ± .006	.831 ± .006	.833 ± .006
Conformal	R-Cov	.887 ± .006	.895 ± .006	.902 ± .006	.908 ± .005	.878 ± .006	.885 ± .006	.891 ± .006	.896 ± .005	.904 ± .005	.912 ± .005	.918 ± .005	.923 ± .004
	APS	1.36 ± .03	1.33 ± .03	1.30 ± .02	1.28 ± .02	1.25 ± .03	1.23 ± .03	1.21 ± .02	1.20 ± .02	1.14 ± .02	1.13 ± .02	1.12 ± .02	1.11 ± .02
	SSCV	.066 ± .004	.062 ± .004	.059 ± .003	.056 ± .003	.056 ± .004	.053 ± .003	.050 ± .003	.048 ± .003	.041 ± .003	.038 ± .003	.036 ± .003	.034 ± .002
	P-Cov	.864 ± .006	.871 ± .006	.877 ± .005	.882 ± .005	.882 ± .006	.891 ± .006	.898 ± .005	.902 ± .005	.896 ± .005	.903 ± .005	.908 ± .005	.912 ± .004
	Acc.	66.8 ± .7%	68.4 ± .7%	69.9 ± .6%	71.0 ± .6%	69.2 ± .7%	7.6 ± .6%	71.9 ± .6%	72.8 ± .6%	71.6 ± .6%	72.8 ± .6%	73.7 ± .5%	74.4 ± .5%
Risk	.108 ± .005	.102 ± .005	.096 ± .004	.091 ± .004	.118 ± .005	.111 ± .005	.105 ± .004	.101 ± .004	.101 ± .004	.097 ± .004	.094 ± .004	.092 ± .004	

Table 13: Calibration size sensitivity (Llama-3-8B, TriviaQA).

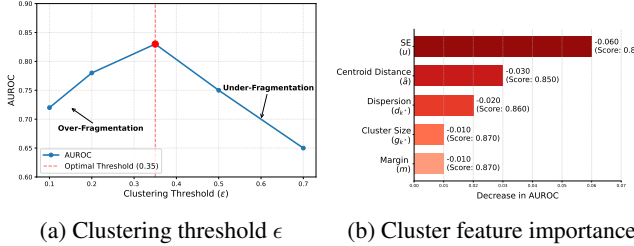


Figure 5: Sensitivity analysis on clustering threshold ϵ and cluster robustness features (via a leave-one-out ablation study).

Weight Setting	AUROC	FPR@95	FPR@90	AUPR	AUARC
Uniform	.857 ± .005	.357 ± .010	.307 ± .009	.835 ± .005	.828 ± .005
Entropy	.861 ± .005	.351 ± .009	.302 ± .009	.838 ± .005	.831 ± .005
Geometry	.859 ± .005	.353 ± .009	.304 ± .009	.837 ± .005	.830 ± .005
Support	.853 ± .006	.362 ± .010	.312 ± .009	.832 ± .006	.825 ± .006
Margin	.855 ± .005	.359 ± .010	.309 ± .009	.834 ± .005	.827 ± .005

Table 14: Discrimination sensitivity over brittleness weighting (Llama-3-8B, TriviaQA).

controlled prioritization over features. Thus, we additionally conduct an ablation on the weight sensitivity in five settings: *Uniform* $\langle \frac{1}{5}, \frac{1}{5}, \frac{1}{5}, \frac{1}{5}, \frac{1}{5} \rangle$, *Entropy* $\langle \frac{2}{6}, \frac{1}{6}, \frac{1}{6}, \frac{1}{6}, \frac{1}{6} \rangle$, *Geometry* $\langle \frac{1}{7}, \frac{2}{7}, \frac{2}{7}, \frac{1}{7}, \frac{1}{7} \rangle$, *Support* $\langle \frac{1}{6}, \frac{1}{6}, \frac{1}{6}, \frac{2}{6}, \frac{1}{6} \rangle$, and *Margin* $\langle \frac{1}{6}, \frac{1}{6}, \frac{1}{6}, \frac{1}{6}, \frac{2}{6} \rangle$, to evaluate robustness under different reasonable weight choices.

As reported in Table 14, ACSE remains stable under all tested weight settings on both TriviaQA and SamSum. On SamSum AUROC ranges from 0.796 to 0.803 and FPR@95 from 0.448 to 0.461. Entropy and Geometry provide slight improvements on some metrics, but the differences are small overall. This suggests that ACSE’s discrimination and safety gains do not depend on a fragile or narrowly tuned weighting choice. A similar pattern holds for the conformal metrics. As also reported in Table 15, on TriviaQA prompt coverage stays within 0.908 to 0.913 and selective risk within 0.091 to 0.095 across all settings, while on SamSum prompt coverage ranges from 0.901 to 0.906 and risk from 0.093 to 0.097. APS and SSCV also change only marginally. Although Entropy and Geometry are slightly favorable on a few metrics, Uniform remains consistently competitive. These results indicate that ACSE is robust to moderate changes in the brittleness weight vector, and its gains do not rely on fragile hyperparameter tuning.

Weight Setting	TriviaQA					SamSum						
	R-Cov	APS	SSCV	P-Cov	Acc.	Risk	R-Cov	APS	SSCV	P-Cov	Acc.	Risk
Uniform	0.920	1.10	0.035	0.911	73.9%	0.093	0.909	1.14	0.040	0.904	72.2%	0.095
Entropy	0.922	1.11	0.034	0.913	73.3%	0.091	0.910	1.15	0.039	0.905	72.0%	0.093
Geometry	0.921	1.09	0.033	0.912	73.7%	0.092	0.912	1.13	0.038	0.906	72.5%	0.094
Support	0.917	1.12	0.037	0.908	72.9%	0.095	0.906	1.16	0.042	0.901	71.8%	0.097
Margin	0.918	1.11	0.036	0.909	73.1%	0.094	0.907	1.15	0.041	0.902	71.9%	0.096

Table 15: Conformal metrics sensitivity over brittleness weighting at $\alpha = 0.10$.

Encoder	AUROC	FPR@95	FPR@90	AUPR	AUARC
All-MiniLM	0.857 ± 0.005	0.357 ± 0.010	0.307 ± 0.009	0.835 ± 0.005	0.828 ± 0.005
MPNet	0.860 ± 0.005	0.352 ± 0.009	0.303 ± 0.009	0.838 ± 0.005	0.831 ± 0.005
E5	0.855 ± 0.005	0.360 ± 0.010	0.310 ± 0.009	0.833 ± 0.005	0.826 ± 0.005
BGE	0.858 ± 0.005	0.355 ± 0.010	0.306 ± 0.009	0.836 ± 0.005	0.829 ± 0.005

Table 16: Encoder Choice Sensitivity (Llama-3-8B, TriviaQA).

Encoder	TriviaQA					SamSum						
	R-Cov	APS	SSCV	P-Cov	Acc.	Risk	R-Cov	APS	SSCV	P-Cov	Acc.	Risk
MiniLM	0.920	1.10	0.035	0.911	73.9%	0.093	0.909	1.14	0.040	0.904	72.2%	0.095
MPNet	0.922	1.09	0.034	0.913	74.2%	0.091	0.912	1.12	0.038	0.907	72.6%	0.093
E5	0.918	1.11	0.036	0.910	73.7%	0.094	0.907	1.15	0.041	0.903	72.0%	0.096
BGE	0.921	1.09	0.034	0.912	74.1%	0.092	0.911	1.12	0.038	0.906	72.5%	0.093

Table 17: Encoder Choice Sensitivity Analysis at $\alpha = 0.10$.

Sentence Encoder Sensitivity. Encoder quality can affect discriminative performance, but not conformal validity which only requires the same deterministic scoring pipeline in calibration and inference. We conduct an ablation on different sentence encoders based on discriminative performance and conformal analysis. ACSE relies only on a semantically meaningful similarity geometry, while soft assignments reduce brittleness near cluster boundaries. As reported in Table 16, ACSE remains stable across all tested sentence encoders on both TriviaQA and SamSum. MPNet achieves the strongest overall discrimination performance, with AUROC of 0.803 on SamSum, but the gains over the MiniLM default are small, amounting to only 0.004, respectively. BGE remains very close to MPNet, while E5 is slightly weaker across most metrics. A similar pattern is observed in Table 17 for the conformal metrics. MPNet and BGE provide slightly stronger conformal performance, but MiniLM remains highly competitive, with only small absolute differences such as about 0.002 in P-Cov and 0.002 in Risk relative to the strongest encoder settings. These results indicate that ACSE is robust to moderate changes in the sentence encoder, and that its gains do not depend on a narrowly chosen embedding backbone.